Electronic Supplementary Material (ESI) for Sustainable Energy & Fuels.

Supporting Information

Tuning B-N Pairs in Porous Carbon Nanorods for Electrochemical Conversion of CO_2 to Syngas with Controllable CO/H_2 Ratios

Xinyue Ma [1], Lei Shi [1], Lipeng Zhang, Chuangang Hu *, Dong Liu*

State Key Laboratory of Organic−Inorganic Composites, Beijing Advanced Innovation Center for Soft Matter Science and Engineering, College of Chemical Engineering, Beijing University of Chemical Technology, Beijing 100029, China

[1] These authors contributed equally

* Corresponding author

chuangang.hu@mail.buct.edu.cn; liudong@mail.buct.edu.cn

Supplemental Experimental Data

Crystal data for BIF-24: $C_{48}H_{64}B_4N_{24}Zn_3$, M_r=1216.64, cubic, a=b=c=20.4868(3) Å, V=8598.5(2) Å^3, T=173 (2) K, space group I3d, Z=4, 977 reflections measured, 741 independent reflections (R_{int}=0.0450). The final *R1* value was 0.0746 (I>2σ(I)). The final *wR(F²)* value was 0.2014 (I>2(I)). The goodness of fit on F^2 was 1.328. CCDC 931167 (BIF-24) contain the supplementary crystallographic data for this paper. These data can be obtained free of charge from The Cambridge Crystallographic Data Centre via www.ccdc.cam.ac.uk/data_request/cif.

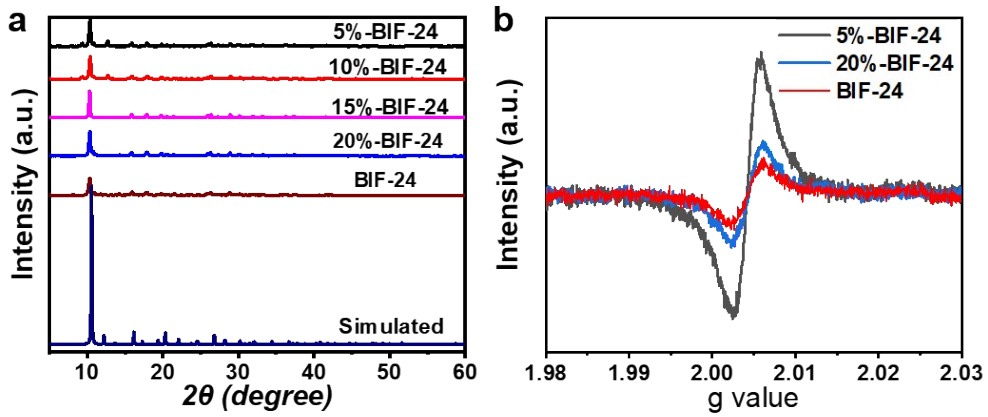

Figure S1. a) Powder XRD patterns of BIF-24 and X-BIF-24, b) The EPR spectrum of 5%-BIF-24, 20%-BIF-24, and BIF-24.

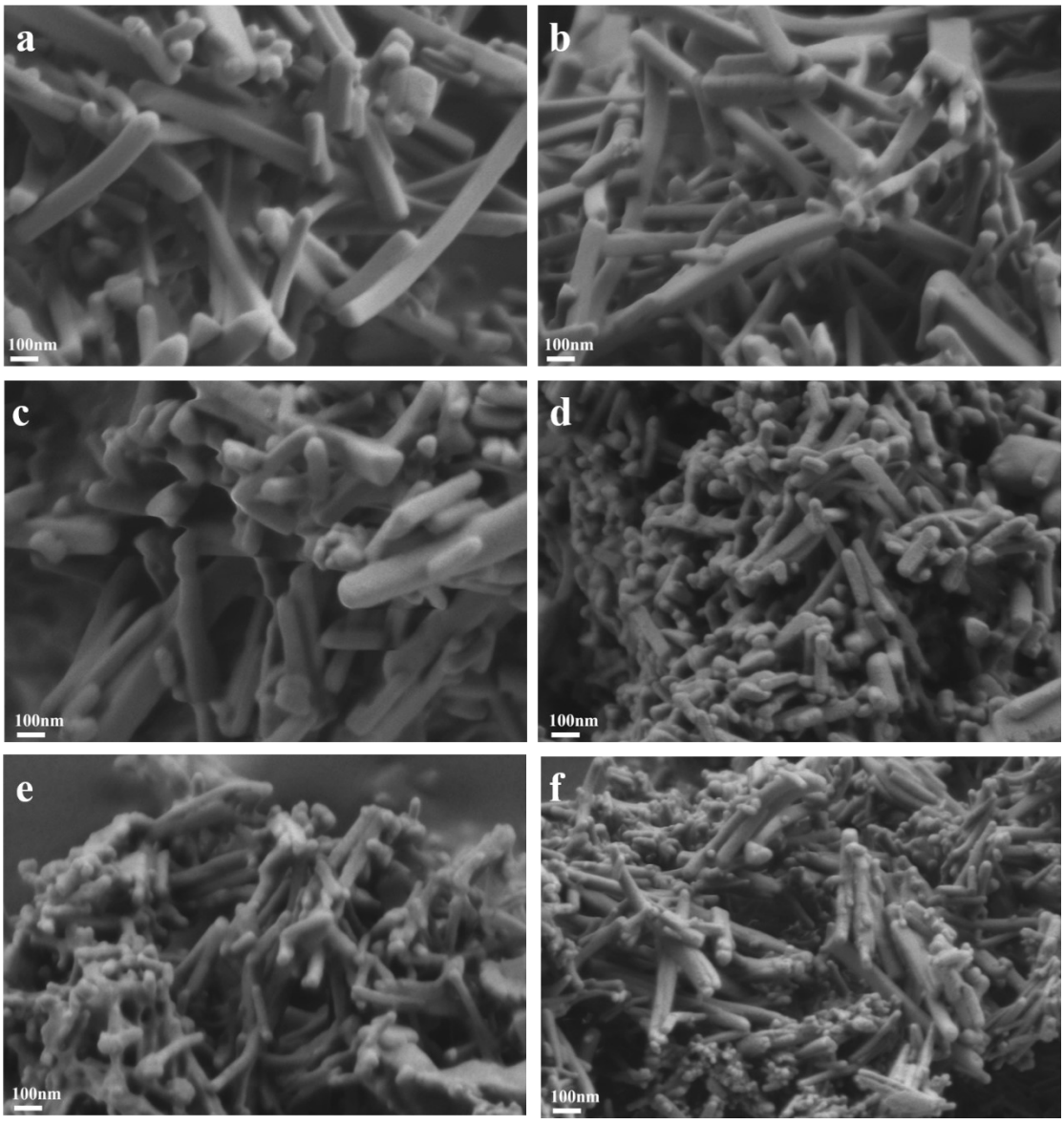

Figure S2. a-e) SEM images of 5%-BIF-24, 10%-BIF-24, 15%-BIF-24, 20%-BIF-24, BIF-24, f) The precursor of NC.

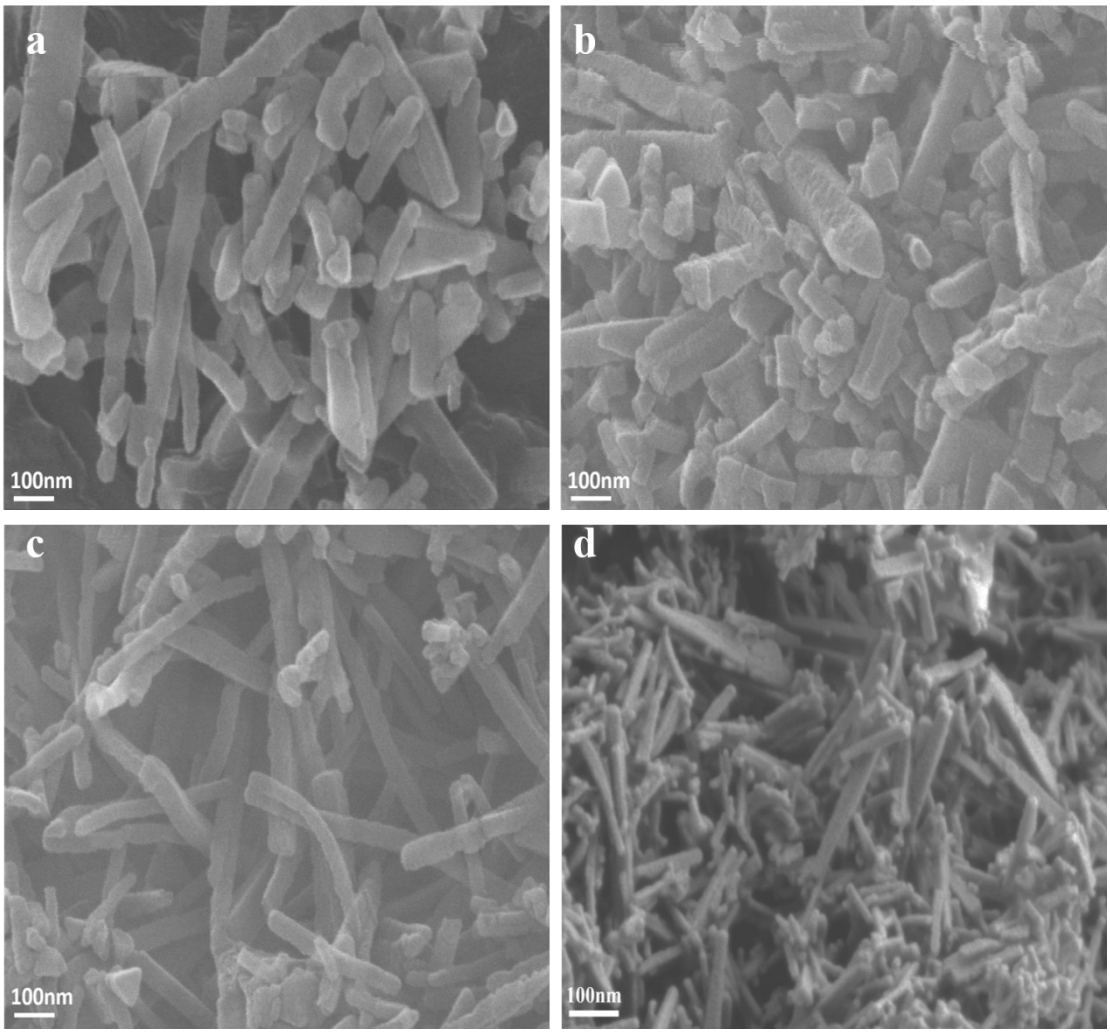

Figure S3. a-c) SEM images of NBC-10%, NBC-15%, NBC-20% and NC.

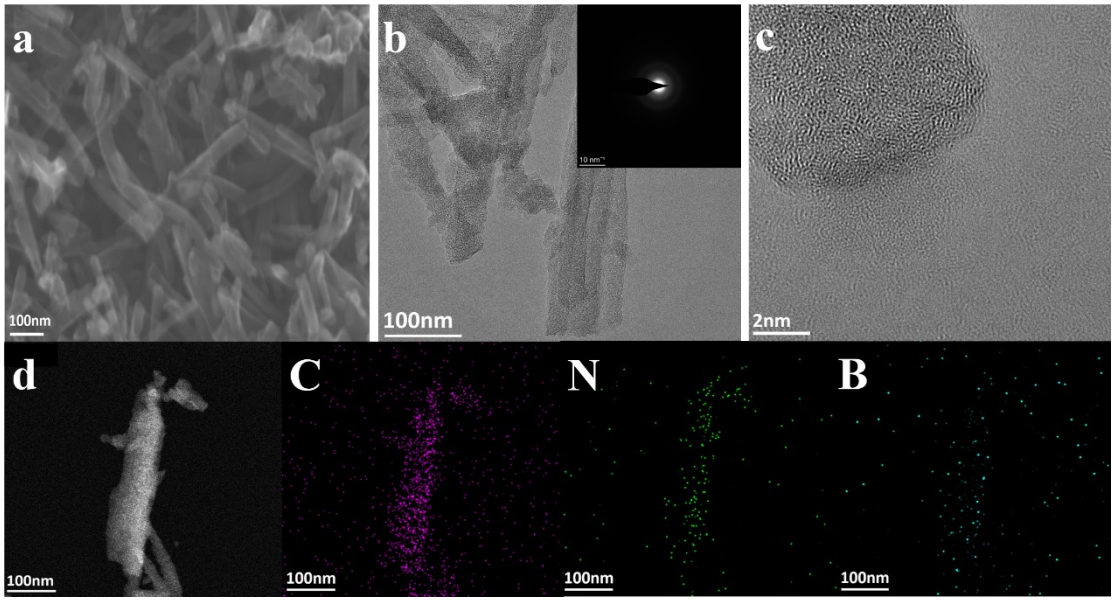

Figure S4. a) SEM image. b) TEM image. c) High-resolution TEM image. d) HAADF image and corresponding elemental mappings of NBC.

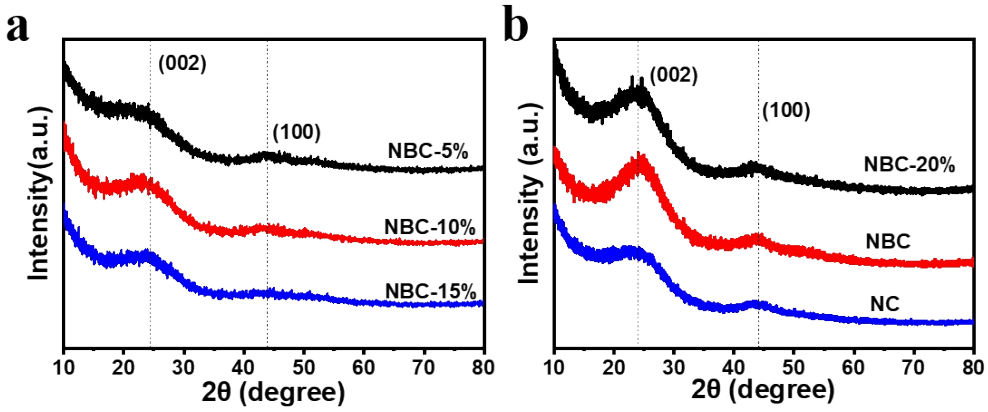

Figure S5. XRD patterns of catalysts.

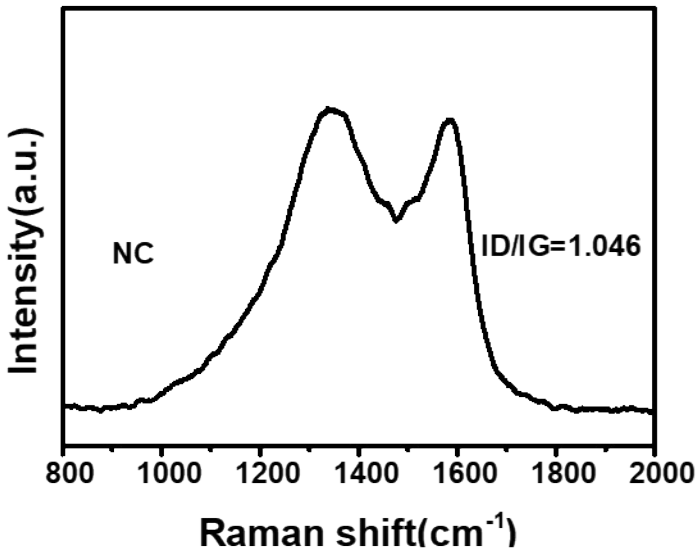

Figure S6. Raman pattern of NC.

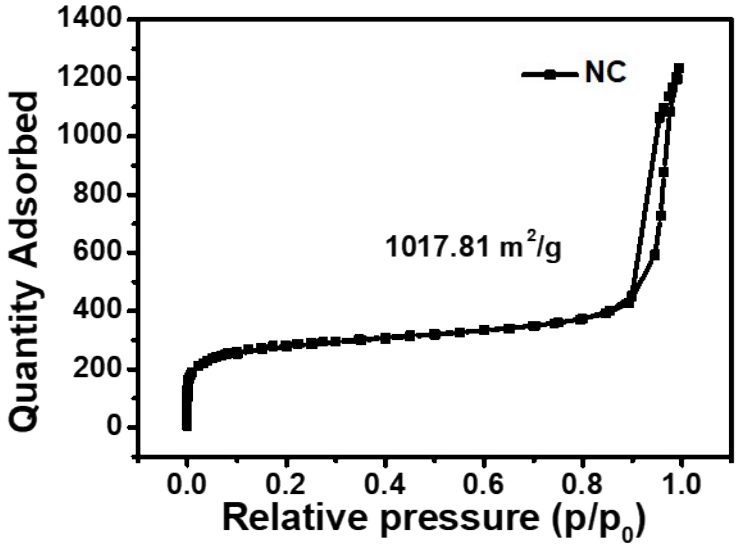

Figure S7. N_2 adsorption-desorption isotherm of NC.

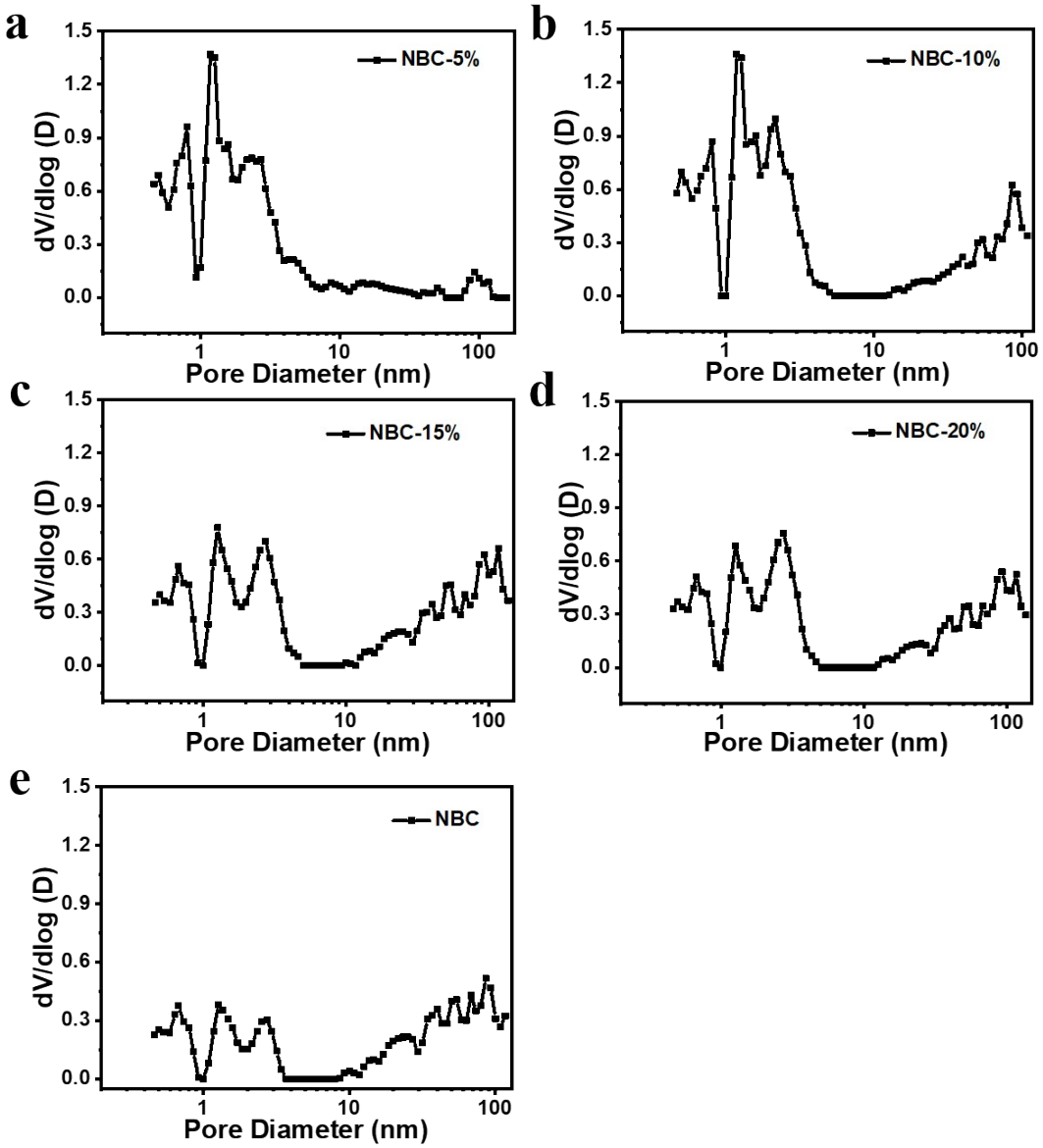

Figure S8. Corresponding pore size distributions of NBCs.

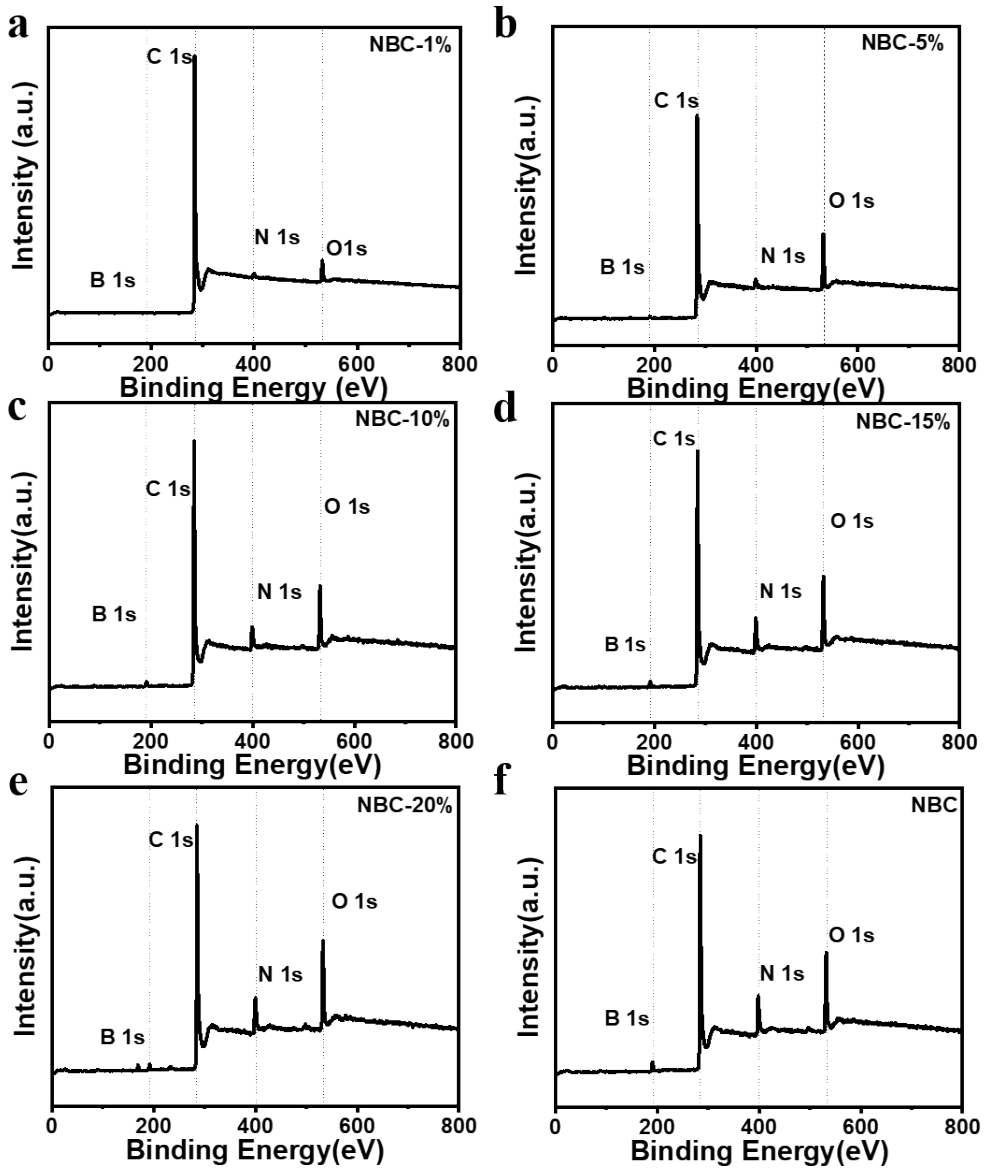

Figure S9. Survey XPS spectra.

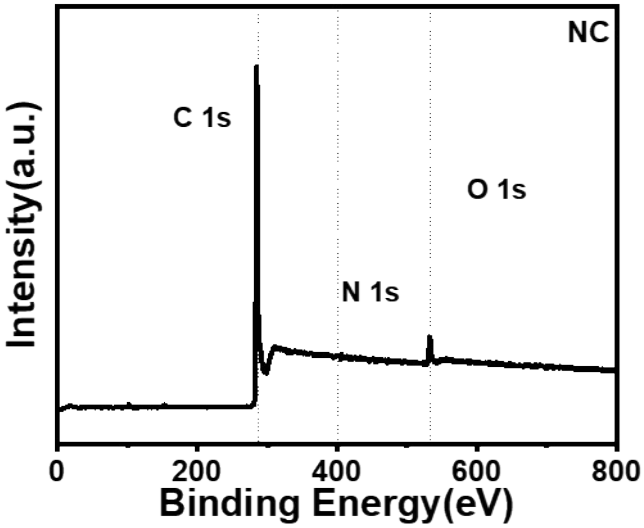

Figure S10. XPS spectrum of NC.

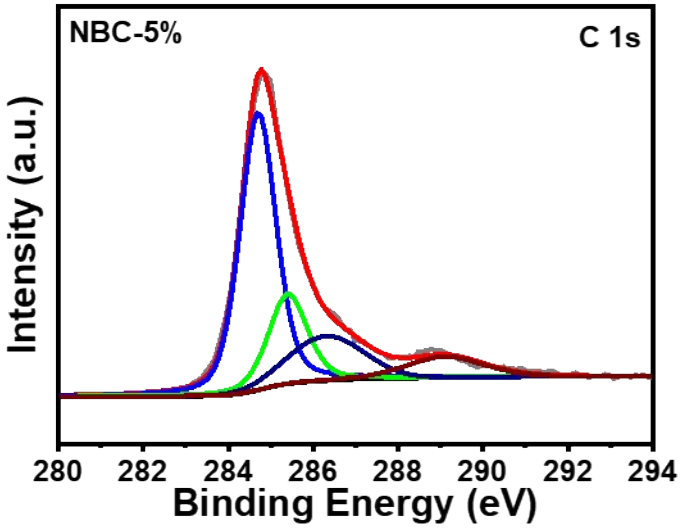

Figure S11. XPS spectra of C 1s of NBC-5%.

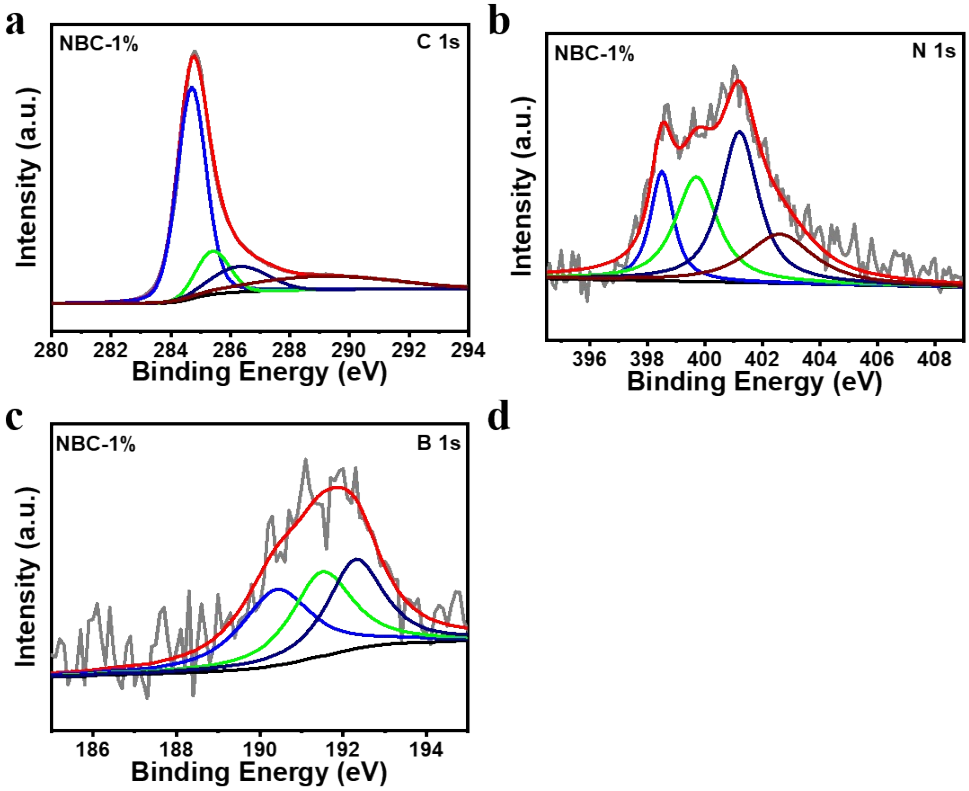

Figure S12. XPS spectra of NBC-1%. a) C 1s, b) N 1s, c) B 1s.

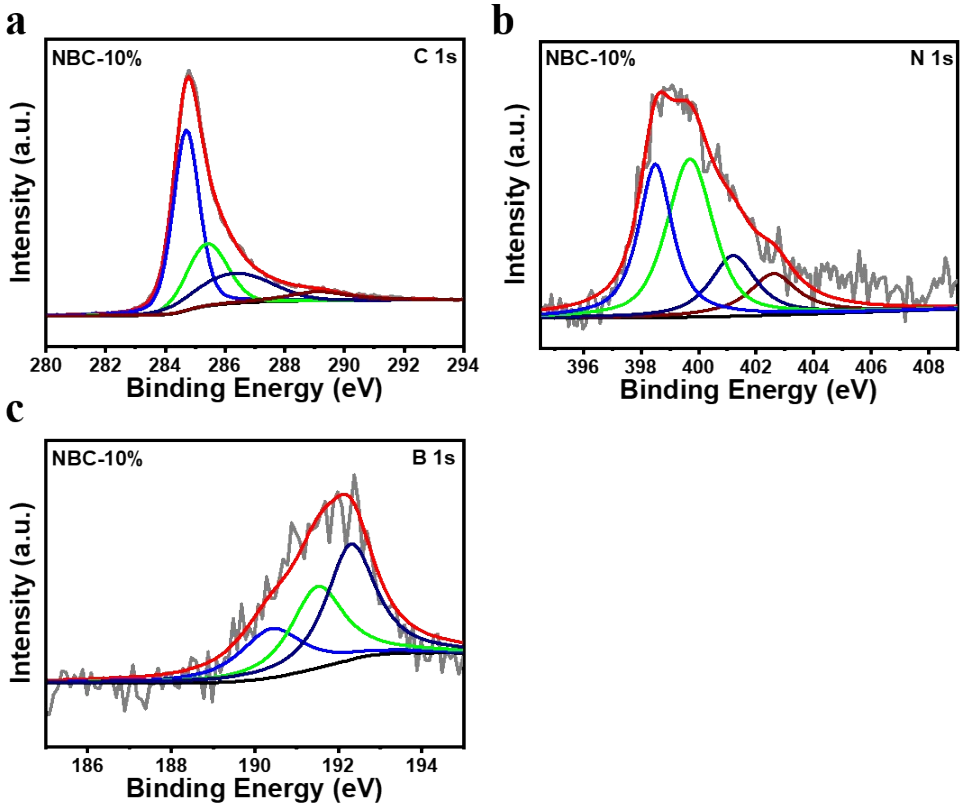

Figure S13. XPS spectra of NBC-10%. a) C 1s, b) N 1s, c) B 1s.

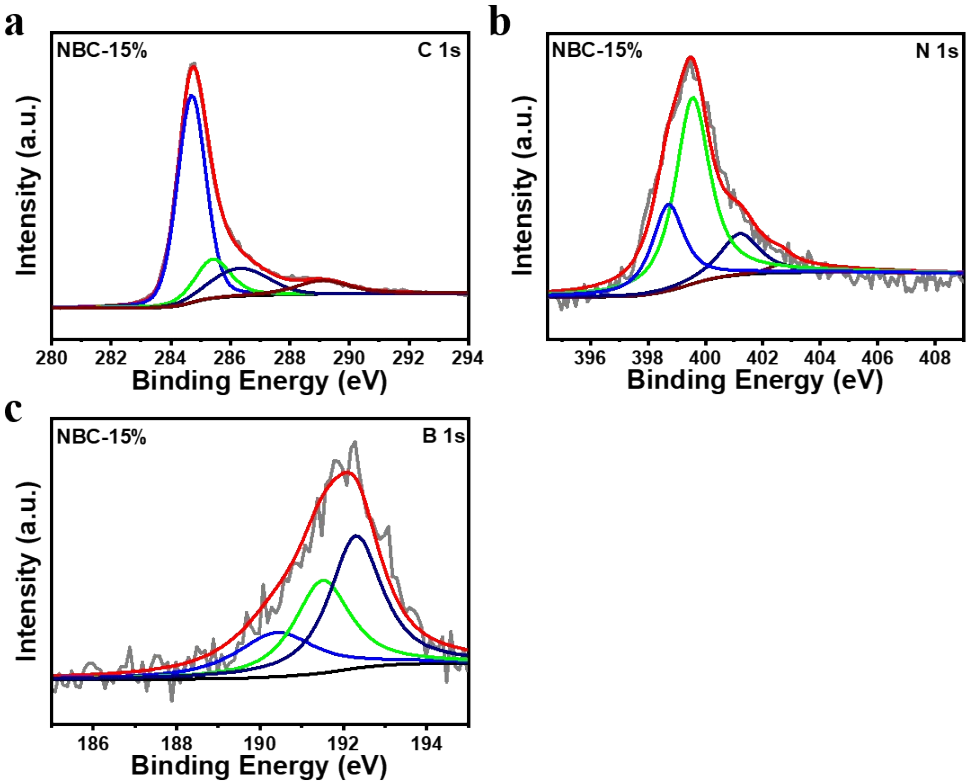

Figure S14. XPS spectra of NBC-15%. a) C 1s, b) N 1s, c) B 1s.

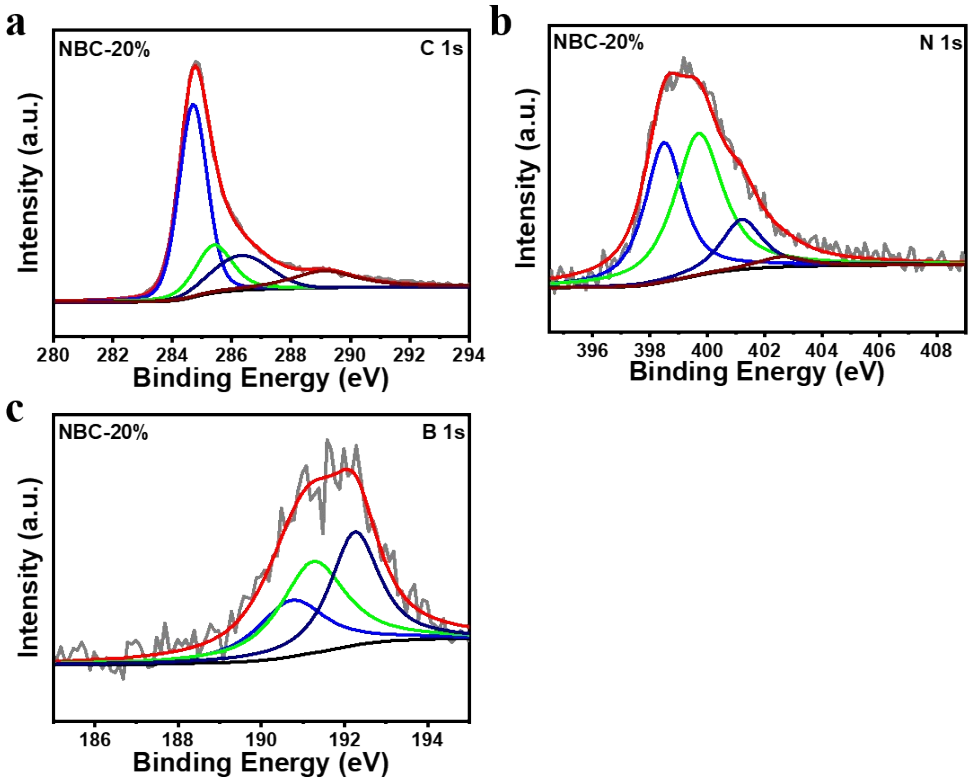

Figure S15. XPS spectra of NBC-20%. a) C 1s, b) N 1s, c) B 1s.

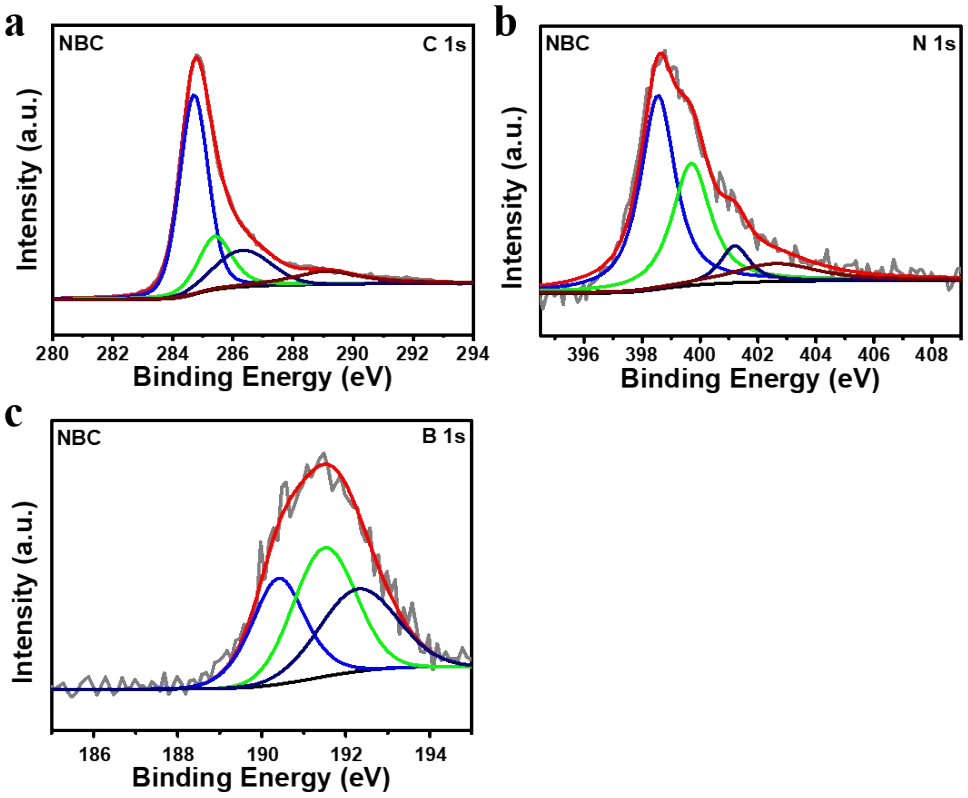

Figure S16. XPS spectra of NBC. a) C 1s, b) N 1s, c) B 1s.

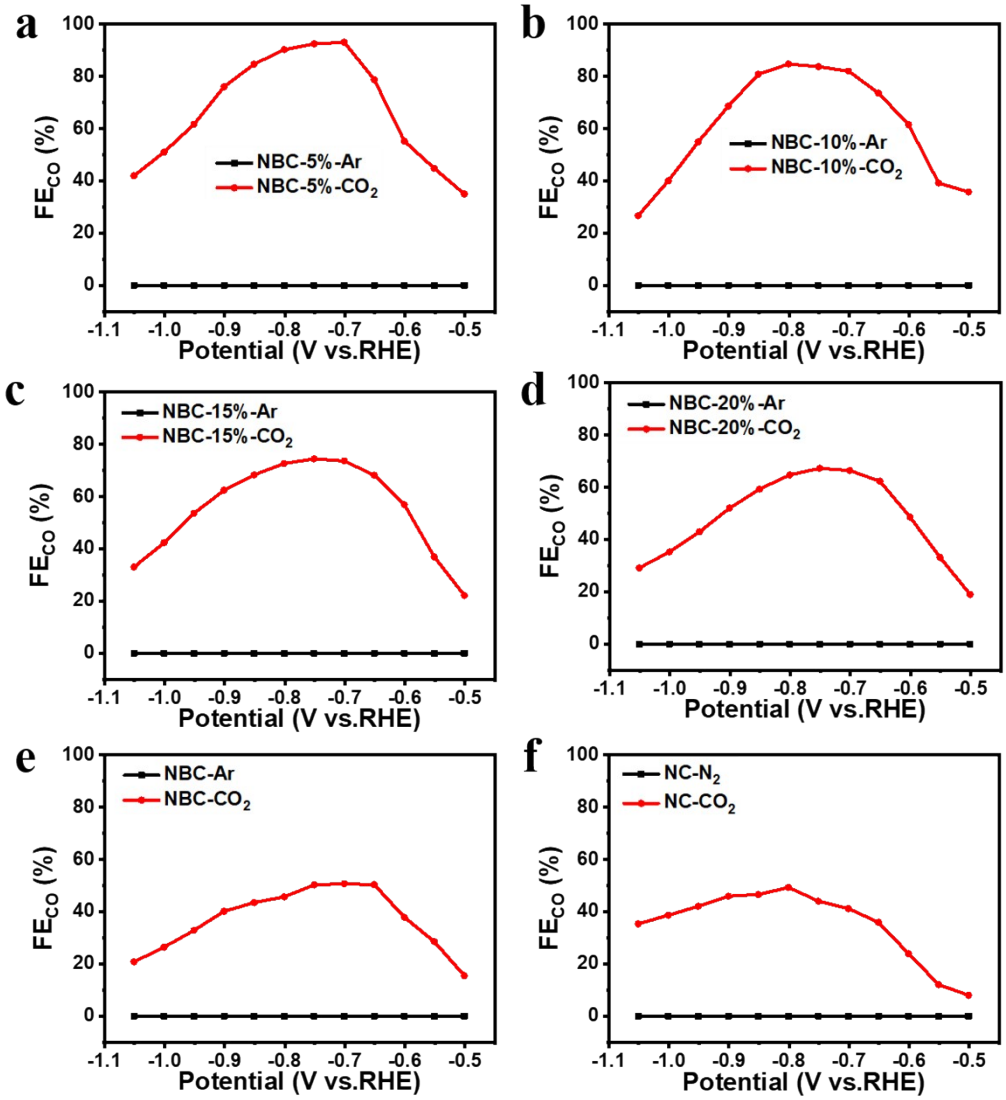

Figure S17. FE of CO on various catalysts in the CO_2-saturated and Ar-saturated 0.1 M $KHCO_3$.

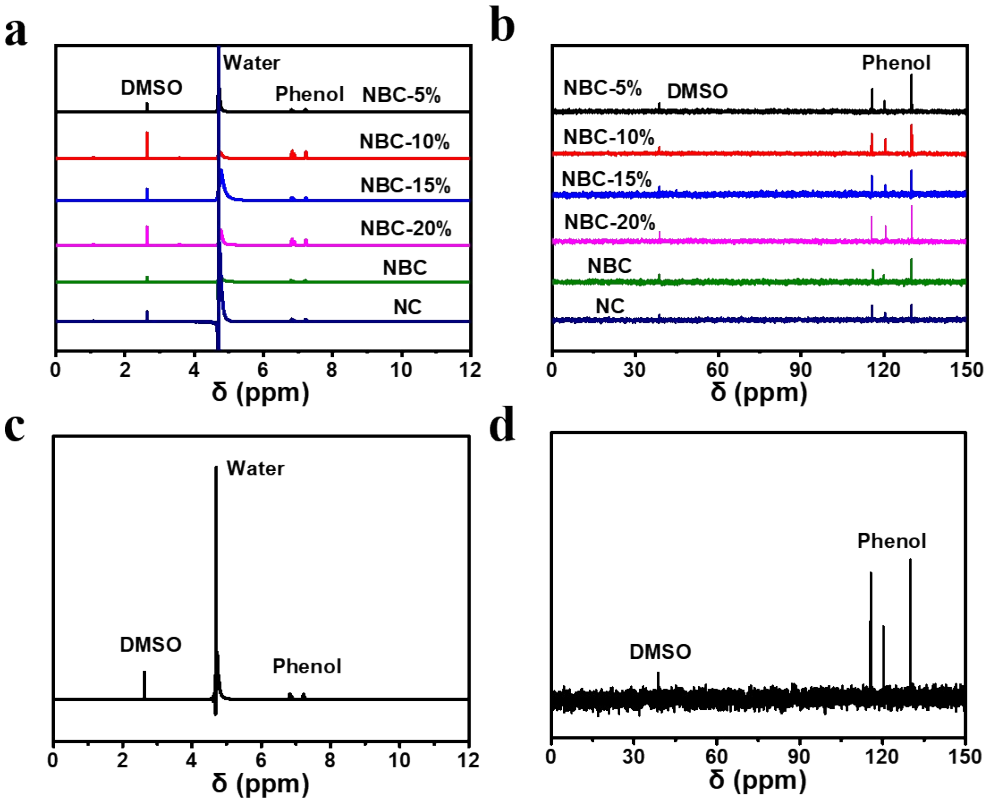

Figure S18. ^{1}H NMR and ^{12}C NMR spectra of a liquid sample (a-b) after CO_2 electroreduction electrolysis (c-d) a blank 0.1 M $KHCO_3$ solution.

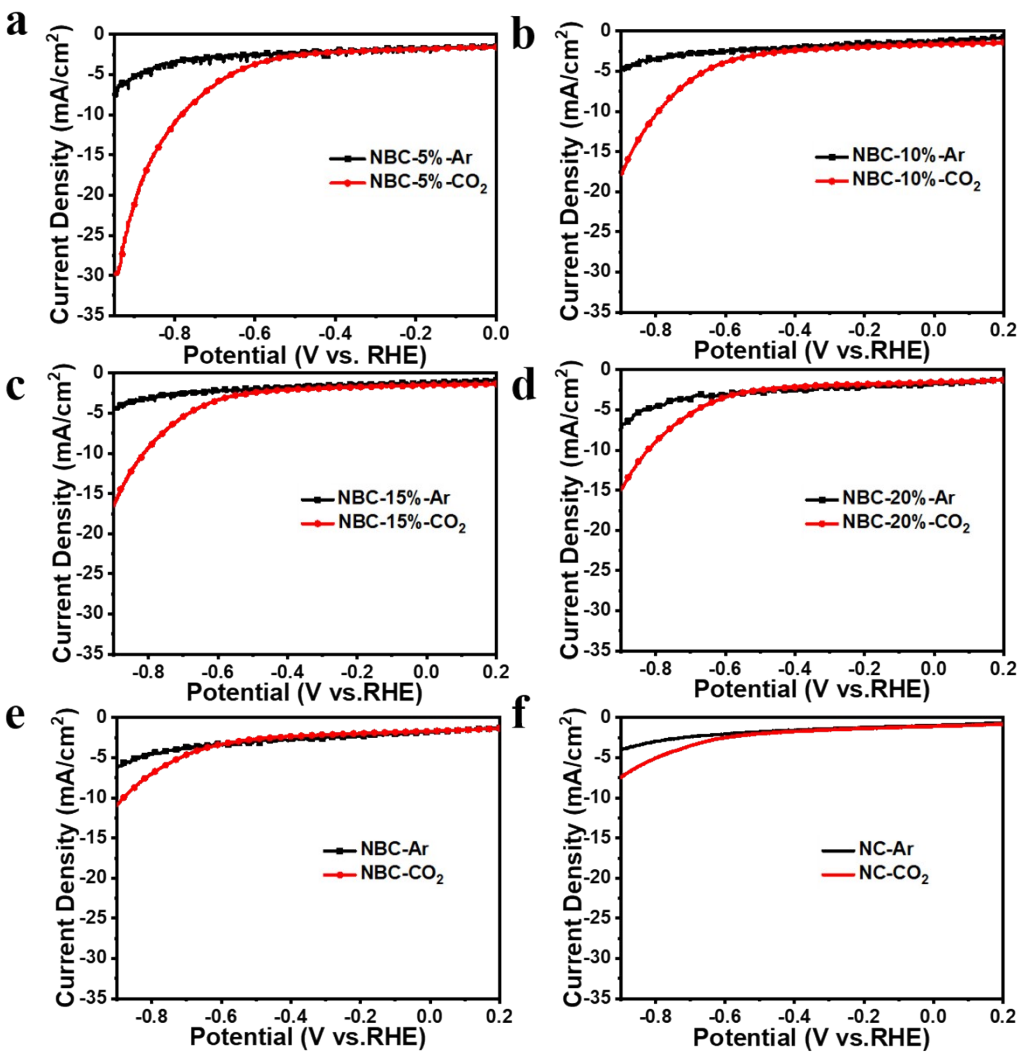

Figure S19. a-f) LSV scans in 0.1 M $KHCO_3$ with CO_2 or Ar atmosphere of NBC-5%, NBC-10%, NBC-15%, NBC-20%, NBC, NC.

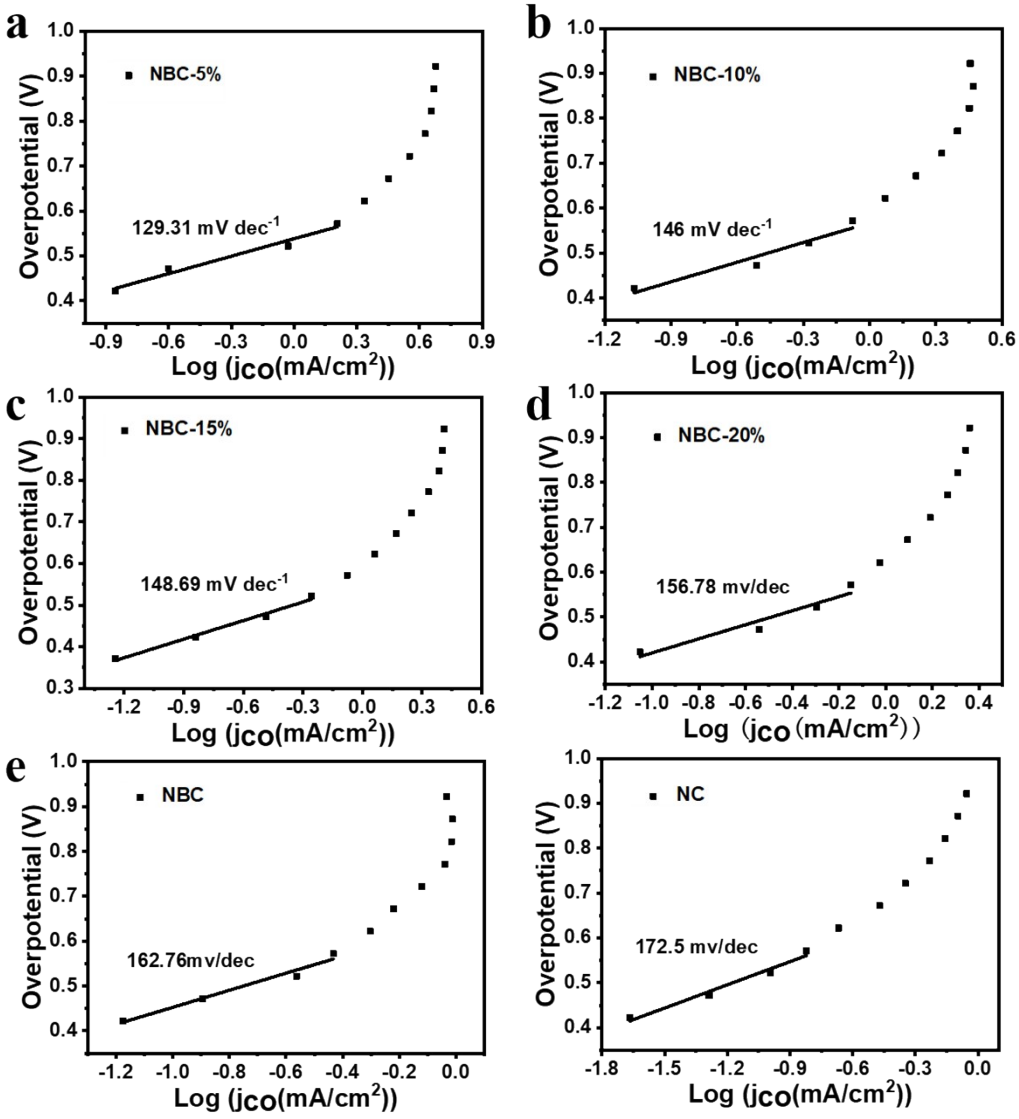

Figure S20. a-f) Tafel plots of various catalysts.

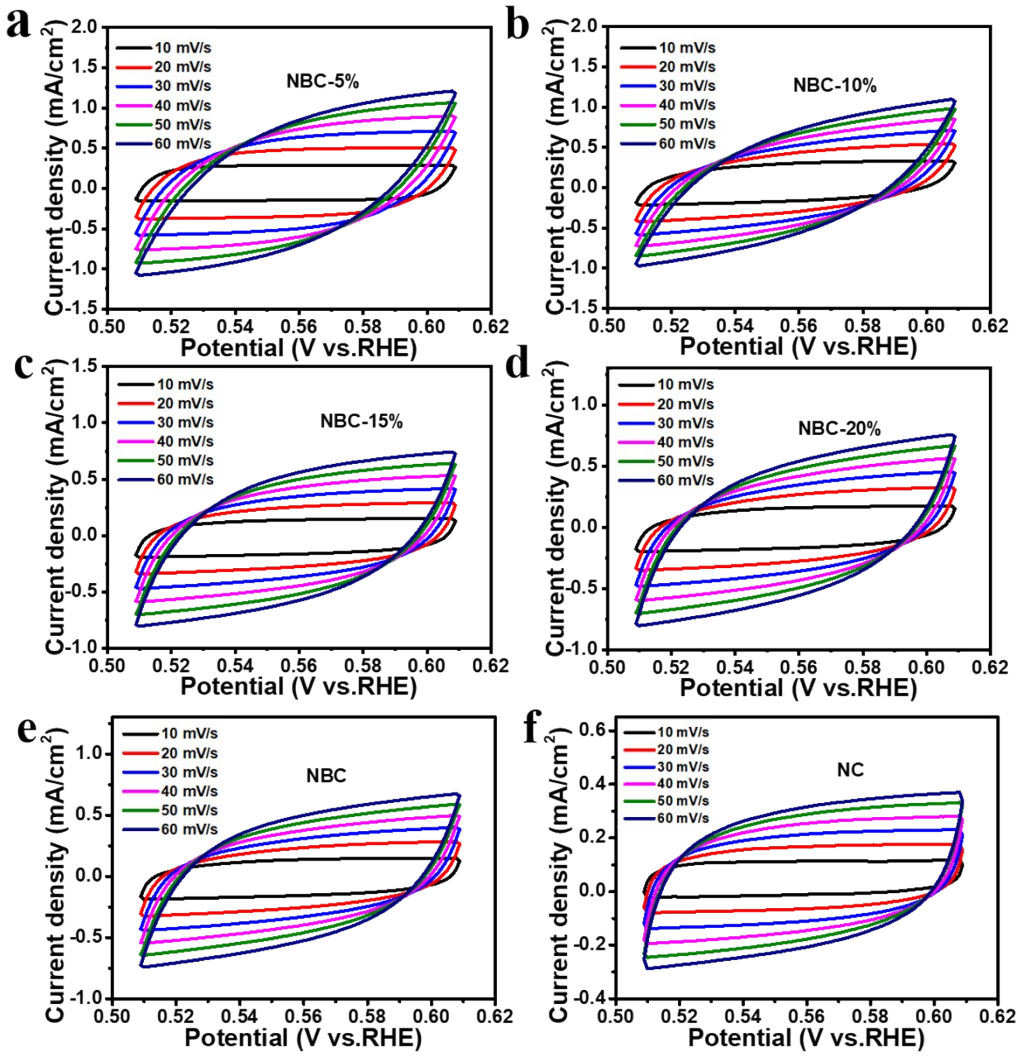

Figure S21. a-f) Current density plots against potentials under a series scan rates. The scan rate: 5, 10, 20, 40 and 60 mV s^{-1}.

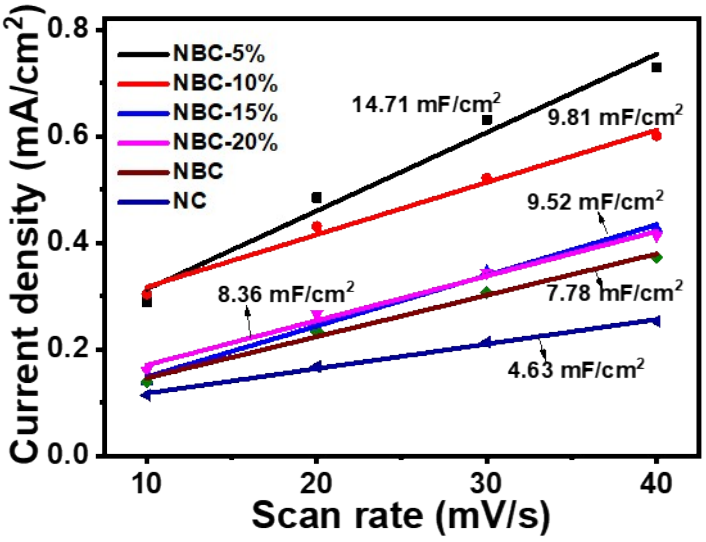

Figure S22. Charging current density differences plotted against the scan rates of catalysts.

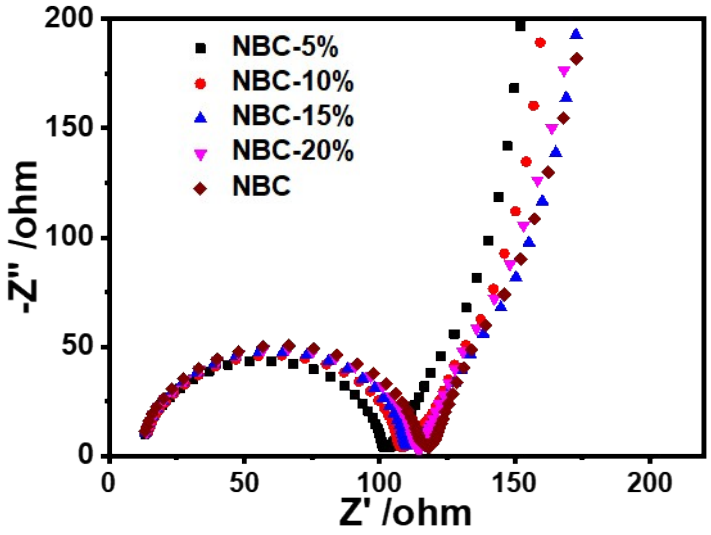

Figure S23. The electrochemical impedance spectroscopy (EIS) analysis of NBCs.

The EIS was conducted from 0.01 Hz to 1 MHz to evaluate the conductivity and electronic transfer kinetics of X-NBC. The diameter of semicircle was changed with the order of NBC-5% < NBC-10% < NBC-15% < NBC-20% < NBC. NBC showed a largest diameter, suggesting the unfavorable electron transfer and conductivity after the increasing in boron and nitrogen. The NBC-5% possessed smaller diameter of the semicircle in the high frequency, indicating the enhanced conductivity and electronic transfer kinetics, which could be owing to the small amounts of boron dopant and the coexistence of nitrogen.

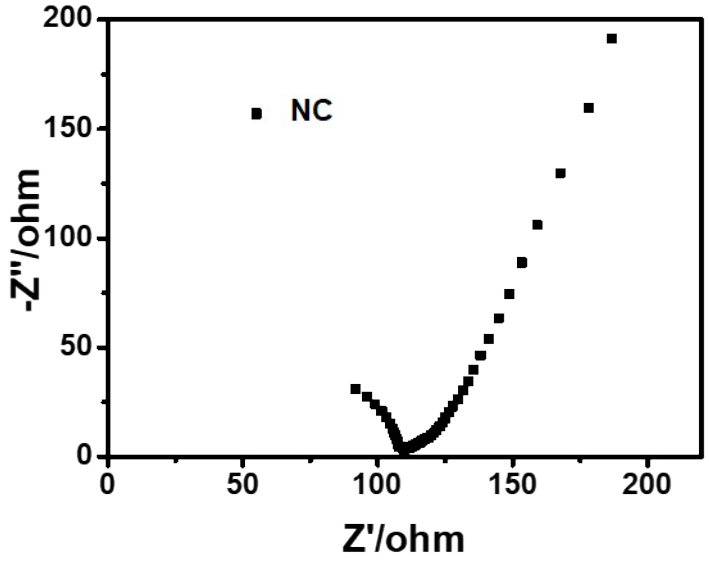

Figure S24. The electrochemical impedance spectroscopy (EIS) analysis of NC.

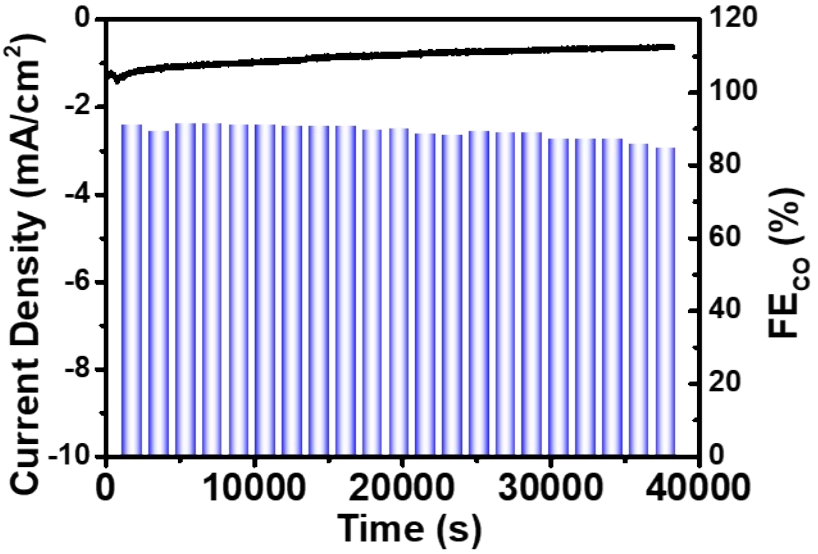

Figure S25. The comparison of CA scans and calculated FE_{CO} for NBC-5%.

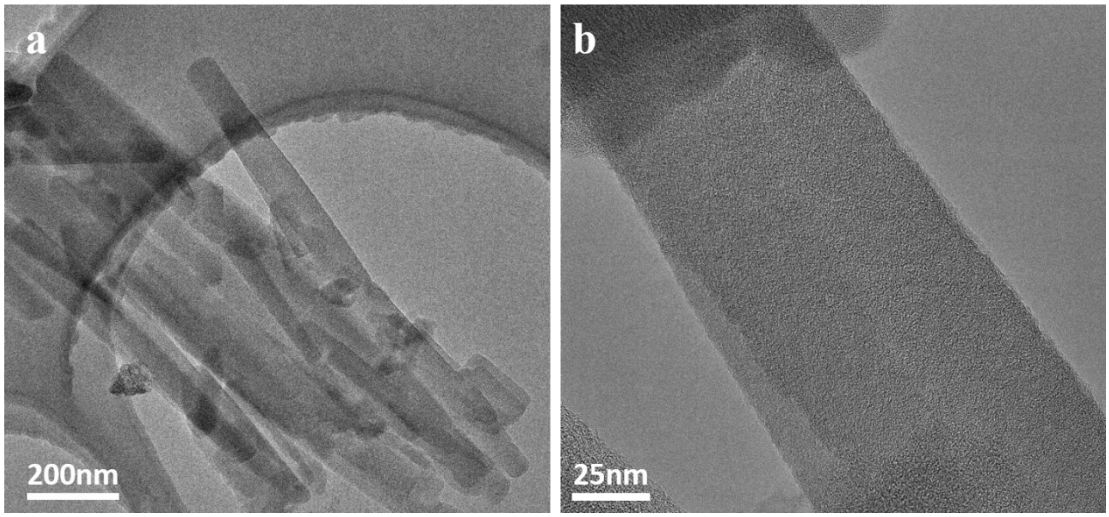

Figure S26. a) TEM image, b) High-resolution TEM image of the NBC-5% after electrolysis.

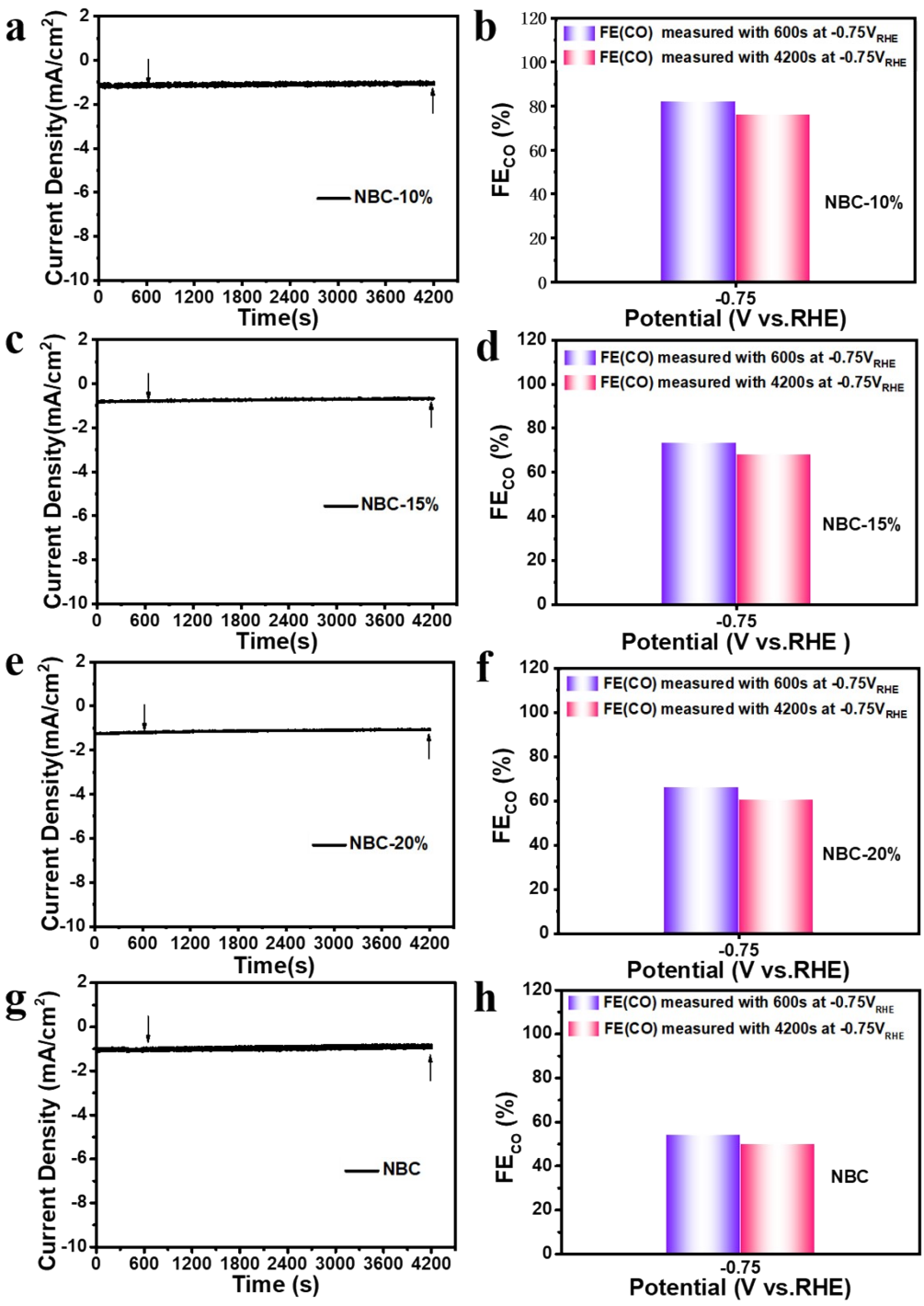

Figure S27. The comparison of CA scans and calculated FE_{CO} for NBC-10%, NBC-15%, NBC-20%, NBC at -0.75 V vs.RHE.

Table S1. Surface Composition of NBC-1%, NBC-5%, NBC-10%, NBC-15%, NBC-20%, NBC and NC.

Sample	C atom%	N atom%	B atom%	O atom%
NBC-1%	93.09	1.99	0.57	4.35
NBC-5%	82.04	4.78	3.06	10.12
NBC-10%	78.26	7.45	5.06	9.22
NBC-15%	75.18	8.92	5.34	10.56
NBC-20%	71.69	10.06	6.32	11.92
NBC	70.5	10.61	8.62	10.28
NC	94.31	1.63	-	4.06

Table S2. The relative content of four major N species.

Sample	**398.5 eV** （**pyridinic N**）	**399.7 eV** **(pyrrolic N)**	**401.2 eV** **(graphite N)**	**402.6 eV** **(oxidized N)**
NBC-1%	0.31406	0.55090	0.71423	0.41080
NBC-5%	1.72382	1.16644	0.86620	1.02354
NBC-10%	2.31661	2.94842	1.23025	0.95473
NBC-15%	2.56642	5.16787	1.32389	0.1626
NBC-20%	3.65122	4.67965	1.39621	0.33292
NBC	5.098168	3.5374	0.822559	1.151875

Table S3. The relative content of B species.

Sample	190.4 eV (C-B)	191.5 eV (C-B-N)	192.3 eV (O-B)
NBC-1%	0.19754	0.18907	0.18339
NBC-5%	0.83831	0.91481	1.30688
NBC-10%	1.19842	1.66447	2.19711
NBC-15%	0.76286	1.76044	2.8167
NBC-20%	2.08908	1.8667	2.36422
NBC	2.92818	3.16889	2.52293

Table S4. Comparison of CO_2RR electrocatalytic performance of NBC-5% with some previously reported CO_2RR catalysts.

Catalyst	Electrolyte	Main product [FE%]	Operating Potential	Tafel (mV/dec)	Ref.
5%-NBC	$KHCO_3$ (0.1M)	CO (93.14)	-0.7 V vs. RHE	129.31	This work
CNF	EMIM-BF_4	CO (98%)	-0.573 V vs. SHE		[1] (2013)
BDD	CH_3OH	HCOOH (74%)	-1.7 V vs. Ag/Ag+		[2] (2014)
PEI-NCNT	$KHCO_3$ (0.1M)	HCOOH (87%)	-1.8 V vs. SCE	134	[3] (2014)
B-Graphene	$KHCO_3$ (0.1M)	HCOOH (66%)	-1.4 V vs. SHE		[4] (2015)
NCNT	$KHCO_3$ (0.1M)	CO (80%)	-0.78 V vs. SHE	203	[5] (2015)
NCNT	$KHCO_3$ (0.1M)	CO (80%)	-1.05 V vs. SHE	160	[6] (2015)
N-3D Graphene	$KHCO_3$ (0.1M)	CO (85%)	-0.58 V vs. SHE	222	[7] (2015)
N-Graphene	$KHCO_3$ (0.5M)	HCOOH (73%)	-0.84 V vs. SHE	135	[8] (2016)
N-GQDs	$KHCO_3$ (0.1M)	C_2H_4 (31%)	-0.75V vs. SHE	198	[9] (2016)
Fe-N-C	$NaHCO_3$ (0.1M)	CO (91%)	-0.6 V vs. RHE		[10] (2017)
HNCM/CNT	$KHCO_3$ (0.1M)	HCOOH (81%)	-0.8 V vs. RHE	138	[11] (2017)
Ni-N-C	$KHCO_3$ (0.1M)	CO (85%)	-0.78 V vs. RHE		[12] (2017)
Au/TiNS	$KHCO_3$ (0.5M)	CO (95%)	-0.65 V vs. RHE		[13] (2018)
FCPC	$KHCO_3$ (0.5M)	CO (88.3%)	-1.0 V vs. RHE	130	[14] (2020)

Table S5. Comparison of CO_2 electroreduction to syngas performance of NBCs with some previously reported CO_2RR catalysts.

Catalyst	Electrolyte	CO [FE%]	Operating Potential	Range of VCO/VH2	Ref.
NBCs	0.1 M $KHCO_3$	CO (93.14)	-0.7 V vs. RHE	1~12.3	This work
Cu–In alloys	0.1 M $KHCO_3$	30	-0.9 V vs. RHE	1/18-1/2.6	[15](2017)
MoSeS	$EmimBF_4$	45.2	-1.15 V vs. RHE	1/1	[16](2017)
Fe-N-C	0.1 M $NaHCO_3$	90	-0.6 V vs. RHE	0-4/1	[17](2017)
Pd/C	0.5 M $NaHCO_3$	~50	-0.6 V vs. RHE	1/2~1/1	[18](2017)
Co_3O_4-CDots-C_3N_4	0.5 M $KHCO_3$	89	-0.6 V vs. RHE	0.25~14.3	[19](2017)
Cu/In_2O_3	0.5M $KHCO_3$	68	-0.7 V vs. RHE	1/4-1/0.4	[20](2018)
Zn	0.1 M $KHCO_3$	85	-1.1 V vs. RHE	1/5-2.31/1	[21](2018)
Au/TiNS	0.5 M $KHCO_3$	81.9	-0.65 V vs. RHE	0.22 ~ 4.93	[22](2018)
n^+p-Si/Al_2O_3/AgP_2	0.5 M $KHCO_3$	67	-0.2 V vs. RHE	1/3 to 5/1	[23](2019)
Ag-SnS_2	0.5 M $KHCO_3$	24.9	-0.6 V vs. SHE	1/1	[24](2019)
Pd bimetallic	0.1 M $NaHCO_3$	70	-0.9 V vs. RHE	2.75~0.5	[25](2019)
CoNi-NC	0.5 M	90	-0.5 V vs. RHE	0.23~2.26	[26](2020)

	$KHCO_3$				
F-γ-In_2Se_3/CP	[Bmim]PF_6/MeCN/H_2O	96.5	-2.0 V vs. SHE	1/3-24/1	[27](2020)

References

1. Kumar, B.; Asadi, M.; Pisasale, D.; Sinha-Ray, S.; Rosen, B. A.; Haasch, R.; Abiade, J.; Yarin, A. L.; Salehi-Khojin, A., *Nat. Commun.,* 2013 10.1038/ncomms3819 4, 1-8.

2. Nakata, K.; Ozaki, T.; Terashima, C.; Fujishima, A.; Einaga, Y., *Angew. Chem. Int. Ed.,* 2014 10.1002/ange.201308657 53, 871-874.

3. Zhang, S.; Kang, P.; Ubnoske, S.; Brennaman, M. K.; Song, N.; House, R. L.; Glass, J. T.; Meyer, T. J., *J. Am. Chem. Soc.,* 2014 10.1021/ja5031529 136, 7845-7848.

4. Sreekanth, N.; Nazrulla, M. A.; Vineesh, T. V.; Sailaja, K.; Phani, K. L., *Chem. Commun.,* 2015 10.1039/c5cc06051f 51, 16061-16064.

5. Wu, J.; Yadav, R. M.; Liu, M.; Sharma, P. P.; Tiwary, C. S.; Ma, L.; Zou, X.; Zhou, X.-D.; Yakobson, B. I.; Lou, J.; Ajayan, P. M., *Acs Nano.,* 2015 10.1021/acsnano.5b01079 9, 5364-5371.

6. Sharma, P. P.; Wu, J.; Yadav, R. M.; Liu, M.; Wright, C. J.; Tiwary, C. S.; Yakobson, B. I.; Lou, J.; Ajayan, P. M.; Zhou, X. D., *Angew. Chem. Int. Ed.,* 2015 10.1002/ange.201506062 54, 13701-13705.

7. Wu, J.; Liu, M.; Sharma, P. P.; Yadav, R. M.; Ma, L.; Yang, Y.; Zou, X.; Zhou, X. D.; Vajtai, R.; Yakobson, B. I.; Lou, J.; Ajayan, P. M., *Nano Lett.,* 2016 10.1021/acs.nanolett.5b04123 16, 466-470.

8. Wang, H.; Chen, Y.; Hou, X.; Ma, C.; Tan, T., *Green Chem.,* 2016 10.1039/c6gc00410e 18, 3250-3256.

9. Wu, J.; Ma, S.; Sun, J.; Gold, J. I.; Tiwary, C.; Kim, B.; Zhu, L.; Chopra, N.; Odeh, I. N.; Vajtai, R.; Yu, A. Z.; Luo, R.; Lou, J.; Ding, G.; Kenis, P. J.; Ajayan, P. M., *Nat. Commun.,* 2016 10.1038/ncomms13869 7, 13869.

10. Huan, T. N.; Ranjbar, N.; Rousse, G.; Sougrati, M.; Zitolo, A.; Mougel, V.; Jaouen, F.; Fontecave, M., *ACS Catal.,* 2017 10.1021/acscatal.6b03353 7, 1520-1525.

11. Wang, H.; Jia, J.; Song, P.; Wang, Q.; Li, D.; Min, S.; Qian, C.; Wang, L.; Li, Y. F.; Ma, C.; Wu, T.; Yuan, J.; Antonietti, M.; Ozin, G. A., Angew. Chem. Int. Ed., 2017 10.1002/anie.201703720 56, 7847-7852.

12. Ju, W.; Bagger, A.; Hao, G. P.; Varela, A. S.; Sinev, I.; Bon, V.; Roldan Cuenya, B.; Kaskel, S.; Rossmeisl, J.; Strasser, P., *Nat. Commun.,* 2017 10.1038/s41467-017-01035-z 8, 944.

13. Marques Mota, F.; Nguyen, D. L. T.; Lee, J.-E.; Piao, H.; Choy, J.-H.; Hwang, Y. J.; Kim, D. H., *ACS Catal.,* 2018 10.1021/acscatal.8b00647 8, 4364-4374.

14. Chen, C.; Sun, X.; Yan, X.; Wu, Y.; Liu, H.; Zhu, Q.; Bediako, B. B. A.; Han, B., *Angew. Chem. Int. Ed.,* 2020 10.1002/anie.202004226 59, 11123-11129.

15. Hoffman Z B, Gray T S, Moraveck K B, et al., *ACS Catal.*, 2017 10.1021/acscatal.7b01161 7, 5381-5390.

16. Xu J, Li X, Liu W, et al., *Angew. Chem., Int. Ed.*, 2017 10.1002/anie.201704928 56, 9121-9125.

17. Huan T N, Ranjbar N, Rousse G, et al., *ACS Catal.*, 2017 10.1021/acscatal.6b03353 7, 1520-1525.

18. Sheng W, Kattel S, Yao S, et al., *Energy Environ. Sci.*, 2017 10.1039/c7ee00071e 10, 1180-1185.

19. Guo S, Zhao S, Wu X, et al., *Nat. Commun.*, 2017 10.1038/s41467-017-01893-7 8, 1828.

20. Xie H, Chen S, Ma F, et al., *ACS Appl. Mater. Interfaces*, 2018 10.1021/acsami.8b12747 10, 36996-37004.

21. Qin B, Li Y, Fu H, et al., *ACS Appl. Mater. Interfaces.*, 2018 10.1021/acsami.8b04809 10, 20530-20539.

22. Marques Mota F, Nguyen D L T, Lee J-E, et al., *ACS Catal.*, 2018 10.1021/acscatal.8b00647 8, 4364-4374.

23. Li H, Wen P, Itanze D S, et al., *Nat. Commun.*, 2019 10.1038/s41467-019-13388-8 10, 5724.

24. He R, Yuan X, Shao P, et al., *Small.*, 2019 10.1002/smll.201904882 15, 1904882.

25. Lee J H, Kattel S, Jiang Z, et al., *Nat. Commun.*, 2019 10.1038/s41467-019-11352-0 10, 3724.

26. Yi J D, Xie R, Xie Z L, et al., *Angew. Chem., Int. Ed.*, 2020 10.1002/anie.202010601 59, 23641-23648.

27. Yang D, Zhu Q, Sun X, et al., *Angew. Chem., Int. Ed.*, 2019 10.1002/ange.201914831 59, 2354-2359.